 CMES, vol.11, no.3, pp.131-143, 2006

Analysis of Structure with Material Interface by Meshfree Method

S. Masuda [1] **and H. Noguchi** [1]

Abstract: This paper presents a novel and accurate technique for modeling discontinuous derivatives in meshfree methods, which will be used in the analysis of structures with material interfaces. The novelty lies in the formulation of the Moving Least Squares Approximation (MLSA) scheme where an introduced discontinuous derivative basis function replaces the conventional linear basis function. Furthermore, it is easy to implement this novelty into existing meshfree methods, such as the Element Free Galerkin (EFG) method, which are based on the MLSA scheme. The successful analyses of one and two-dimensional structures with material interfaces demonstrate the potential of the proposed technique.

keyword: Manuscript, Preparation, Typeset, Format, CMES.

1 Introduction

Recent years have seen the rise of a multitude of meshfree methods. Recent methods include Smoothed Particle Hydrodynamics [Monagham (1982)], Diffuse Element Method [Nayroles and Villon (1992)], H-P Clouds [Duarte and Oden (1996)], Reproduced Kernel Particle Methods [Liu and Zhang (1995)], Element Free Galerkin (EFG) Method [Belytschko, Lu and Gu (1994)], Point Interpolation Method [Gu and Liu (2001)] and the Meshless Local Petrov Galerkin Method [Atluri and Zhu (1998)] [Lin and Atluri (2000)]. In depth detail of those methods are described in recent literature [Liu (2002)].

For some meshfree methods, the displacement at a point of evaluation is frequently approximated from the displacements of surrounding nodes by using the Moving Least Squares Approximation (MLSA) scheme [Nayroles and Villon (1992)] [Belytschko, Lu and Gu (1994)] [Atluri and Zhu (1998)] [Dilts (1999)] [Lin and Atluri (2000)]. As a result, it yields continuous displacement fields and continuous displacement derivatives or strains. Therefore, for the analysis of homogeneous problems, it is widely accepted that meshfree methods are more accurate than the finite element method (FEM).

However, practical problems are inhomogeneous problems. Examples include structures composing of different members fabricated from different materials, and composite structures. In the analysis of such problems, a discontinuity of displacement derivatives arises and meshfree methods using MLSA require special treatment to take this discontinuity into account [Cordes and Moran (1996)] [Kawashima and Noguchi (2000)] [Noguchi and Kawashima (2004)] [Krogauz and Belytschko (1998)].

Cordes et al. [Cordes and Moran (1996)] and Kawashima et al. [Kawashima and Noguchi (2000)] [Noguchi and Kawashima (2004)] proposed a patch method where MLSA is utilized independently for both sides (patches) of the material interface. The continuous condition is only imposed on the displacement at the interface by using the Lagrange multiplier method or the penalty method. This approach though very simple, had derivative oscillations around the interface and gave results that were less accurate than FEM. Krongauz et al. [Krogauz and Belytschko (1998)] proposed the Enriched method, which uses a jump shape function on the interface in order to improve accuracy. The method demonstrated better accuracy, however, it was also reported that the jump function must be given in advance and its shape sometimes affects the results. Furthermore, additional degrees of freedom may be necessary to determine the amplitude of the jump function in the global system of equations. Wang et al. [Wang, Chen and Sun (2003)] also proposed the Enriched method using the jump function for the Reproduced Kernel Particle Method. This method requires no additional degrees of freedom, however, the shape of given jump function still affects the results. Li et al. combined the two different types of meshfree methods (MLPG2 and MLPG5) to treat material discontinuity accurately. However, each method utilizes a different theoretical basis and it lacks the consistency of the formulation. [Li; Shen, Han and Atluri (2003)]

Keeping in mind the complexity of practical problems, a

[1] Keio University, Yokohama, Kanagawa, Japan

novel and accurate technique for modeling discontinuous derivatives in meshfree methods is proposed for the analysis of structures with material interfaces. A novel discontinuous derivative basis function replaces the conventional linear basis function in the MLSA scheme. Therefore, it is easy to implement this technique into existing MLSA-based meshfree methods, such as the EFG method.

The outline of this paper is as follows. Section 2 briefly reviews the MLSA scheme. Section 3 will introduce the proposed technique for one-dimensional and two-dimensional problems. Section 4 describes various observations noted regarding the proposed technique. Section 5 will present several numerical examples of one-dimensional and two-dimensional structures to validate the proposed technique. Section 6 will present a conclusion.

2 Moving Least Squares Approximation (MLSA) review

For most current meshfree methods, MLSA is utilized for approximating function values in the displacement field [Nayroles and Villon (1992)] [Belytschko, Lu and Gu (1994)] [Liu (2002)] [Dilts (1999)]. According to Belytschko et al. [Belytschko, Lu and Gu (1994)], the displacement vector $\mathrm{u}^h(\mathbf{x})$ is approximated by a polynomial as shown in Eq.1, where n represents the number of terms in the polynomial. Eq.2 shows the linear basis vector $\mathbf{p}$ and its coefficient vector $\mathbf{a}$ in a two-dimensional domain (n=3).

$$u^h(\mathbf{x}) = \sum_{j=1}^{n} p_j(\mathbf{x}) a_j(\mathbf{x}) \equiv \mathbf{p}^T(\mathbf{x})\mathbf{a}(\mathbf{x}) \tag{1}$$

$$\mathbf{p}^T(\mathbf{x}) = (1,\, x,\, y), \quad \mathbf{a}^T(\mathbf{x}) = (a_1, a_2, a_3) \tag{2}$$

The coefficients in $\mathbf{a}(\mathbf{x})$ are determined by minimizing the weighted functional in Eq.3,

$$J = \sum_{I=1}^{m} w(r_I) \left(u^h(\mathbf{x}_I) - u_I \right)^2, \quad r_I = |\mathbf{x} - \mathbf{x}_I| \tag{3}$$

where u_I is the unknown nodal value of displacement u^h at node $\mathbf{x}_I$, r_I is the distance between two points $\mathbf{x}$ and $\mathbf{x}_I$ and m is the number of nodes in the domain of influence whose radius is ρ. In this paper, the fourth-order polynomial in Eq.4 is adopted as a weight function $w(r)$, which satisfies $w(\mathrm{P}) = 0$, $dw/dr(\rho) = 0$ and $d^2w/\mathrm{d}r^2(\rho) = 0$.

$$w(r_I) = \begin{cases} 1 - 6\left(\frac{r_I}{\rho}\right)^2 + 8\left(\frac{r_I}{\rho}\right)^3 - 3\left(\frac{r_I}{\rho}\right)^4 & (0 \le r_I \le \rho) \\ 0 & (\rho < r_I) \end{cases} \tag{4}$$

The approximated displacement vector $u^h(\mathbf{x})$ can then be expressed as a function of the nodal value u_I as shown in Eqs.5-7,

$$u^h(\mathbf{x}) = \sum_{I=1}^{m} \mathbf{p}^T(\mathbf{x}) \left(\mathbf{A}^{-1}(\mathbf{x})\mathbf{B}(\mathbf{x}) \right)_I u_I = \sum_{I=1}^{m} \phi_I(\mathbf{x}) u_I \tag{5}$$

$$\mathbf{A}(\mathbf{x}) = \sum_{I=1}^{m} w(r_I)\, \mathbf{p}(\mathbf{x}_I)\, \mathbf{p}^T(\mathbf{x}_I) \tag{6}$$

$$\mathbf{B}(\mathbf{x}) = [w(r_1)\mathbf{p}(\mathbf{x}_1),\, w(r_2)\mathbf{p}(\mathbf{x}_2),\, \cdots w(r_m)\mathbf{p}(\mathbf{x}_m)] \tag{7}$$

Where $\phi_I(\mathbf{x})$ corresponds to the shape function used in the finite element method.

3 MLSA with Discontinuous Derivative Basis Function

MLSA is known to yield a continuous displacement field in space, which contains continuous derivatives. However, this continuity of meshfree approximations is sometimes a drawback in problems where derivatives of the exact solution possess discontinuities, such as strain jumps at material interfaces. This paper presents an accurate technique for modeling discontinuous derivatives by introducing a novel discontinuous derivative basis function into the existing MLSA scheme.

3.1 One-Dimensional Problems

Fig. 1 illustrates the concept of the discontinuous derivative basis function technique for one-dimensional problems. A material interface is located at $x = x_d$ and sampling points are scattered on both sides of the interface. A bi-linear basis function, represented by a solid line in Fig. 1, is the adopted discontinuous derivative basis function and replaces the conventional linear basis function (represented by a dotted line) in the existing MLSA scheme. The adopted basis function is continuous at the interface

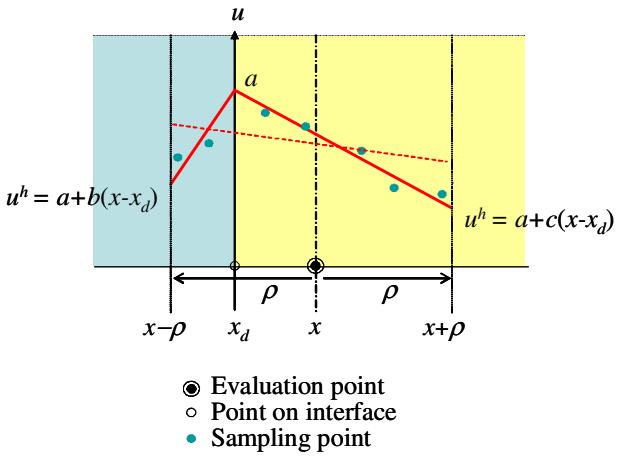

Figure 1 : Discontinuous derivative basis function for 1-D problems

but its slope is different on both sides. In this case, the functions to be minimized are rewritten as Eqs.8, 9,

$$\begin{cases} u^h(x) = a + b\,(x - x_d) & (x \le x_d) \\ u^h(x) = a + c\,(x - x_d) & (x > x_d) \end{cases} \tag{8}$$

$$J = \sum_{I=1}^{n_{d1}} w(r_I)\,(a + b\,(x_I - x_d) - u_I)^2 + \sum_{I=n_{d1}}^{n_{d1}+n_{d2}} w(r_I)\,(a + c\,(x_I - x_d) - u_I)^2 \tag{9}$$

where n_{d1} represents the number of points on the left side of the interface ($x \le x_d$) and n_{d2} on the right ($x > x_d$). Therefore the total number of the sampling points in the domain of influence is $n_{d1} + n_{d2}$. By satisfying the stationary condition of Eq.9 approximates the displacement function in Eq.10.

$$u^h(\mathbf{x}) \equiv \sum_{I}^{n_{d1}+n_{d2}} \phi_I(\mathbf{x}) u_I \tag{10}$$

$$\begin{cases} \phi_I(\mathbf{x}) = \mathbf{P}_1(x)^T \mathbf{A}^{-1} \mathbf{B}_I & (x \le x_d) \\ \phi_I(\mathbf{x}) = \mathbf{P}_2(x)^T \mathbf{A}^{-1} \mathbf{B}_I & (x > x_d) \end{cases} \tag{11}$$

$$\mathbf{A} = \sum_{I=1}^{n_{d1}} w(r_I)\,\mathbf{p}_1(x_I)\,\mathbf{p}_1(x_I)^T + \sum_{I=n_{d1}}^{n_{d1}+n_{d2}} w(r_I)\,\mathbf{p}_2(x_I)\,\mathbf{p}_2(x_I)^T \tag{12}$$

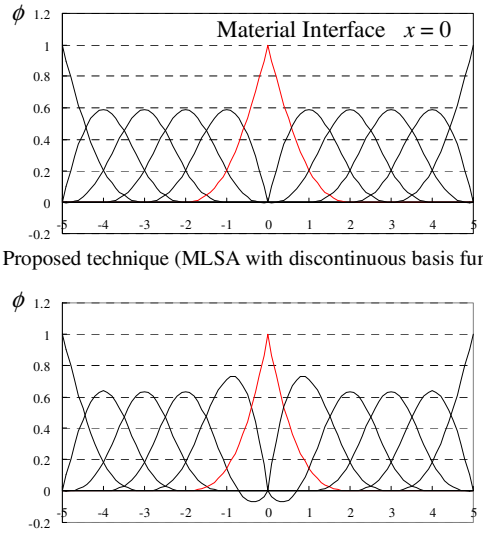

(a) Proposed technique (MLSA with discontinuous basis function)

(b) Method by Wang et al. (Enriched RKF [Wang, Chen and Sun (2003)])

Figure 2 : Shape function around interface (1-D)

$$\mathbf{B}(\mathbf{x}) = [w(r_1)\mathbf{p}(\mathbf{x}_1), \cdots, w(r_{n_{d1}})\mathbf{p}(\mathbf{x}_{n_{d1}}), w(r_{n_{d1}+1})\mathbf{p}(\mathbf{x}_{n_{d1}+1}), \cdots, w(r_{n_{d1}+n_{d2}})\mathbf{p}(\mathbf{x}_{n_{d1}+n_{d2}})] \tag{13}$$

$$\mathbf{u}^T = \{\ u_1 \quad u_2 \quad \ldots \quad u_n\ \} \tag{14}$$

$$\mathbf{p}_1(x) = \begin{bmatrix} 1 \\ x - x_d \\ 0 \end{bmatrix}, \quad \mathbf{p}_2(x) = \begin{bmatrix} 1 \\ 0 \\ x - x_d \end{bmatrix} \tag{15}$$

The shape function obtained by this technique is illustrated in Fig. 2. It is coupled together with the shape function obtained by Wang et al. for comparison [Wang, Chen and Sun (2003)]. Both shape functions appear similar and display a sharp peak, the discontinuous derivative, at the material interface.

3.2 Two-Dimensional Problems

Two-dimensional problems are similar to one-dimensional problems in the sense that two sets of complete linear polynomial functions are considered as shown in Fig. 3. Both linear polynomial functions are reproduced in Eqs.16-17 with Eq.17 representing the shape of the material interface. Eq.17

is also a constraint equation that all points on the interface have to satisfy.

$$\begin{cases} u_A^h = a + b\,(x - x_d) + c\,(y - y_d)\ h(x,y) \ge 0 \\ u_B^h = d + e\,(x - x_d) + f\,(y - y_d)\ h(x,y) < 0 \end{cases} \tag{16}$$

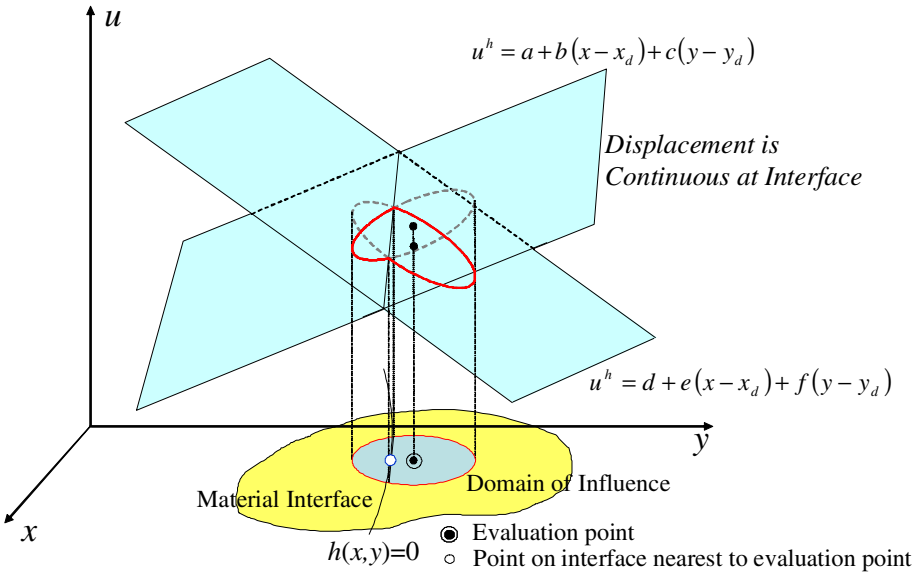

Figure 3 : Discontinuous derivative basis function for 2-D problems (Concept)

$$h(x,y)=0 \tag{17}$$

Subscripts A and$B$ in Eq.16 indicate the separate zones consisting of different materials in the domain of influence. The point $\mathbf{x}_d=(x_d,y_d)$ is nearest to the evaluation point on the interface.

If the shape of the interface is straight as shown in Fig. 4-1 and assuming the interface is not parallel to the y-axis, Eq.17 is simply rewritten as Eq.18.

$$y-y_d=\alpha(x-x_d),\ \alpha\neq 0 \tag{18}$$

The coefficients in Eq.16 are determined such that the intersection of those two functions when projected onto the x-y plane coincides with the interface. For $\mathbf{x}_d$ and $\mathbf{x}_d=(x_d+x',y_d+\alpha x')$ $x'\neq 0$ on the interface, the following equation holds.

$$u_A^h(\mathbf{x}_d)=u_B^h(\mathbf{x}_d),\ u_A^h(\mathbf{x}_d)=u_B^h(\mathbf{x}_d) \tag{19}$$

Thus, the displacement basis function, considering the straight interface in the domain of influence, is approximated in Eq.20.

$$\begin{cases} u_A^h=a+b(x-x_d)+c(y-y_d) & h(x,y)\geq 0 \\ u_B^h=a+\{b+(c-f)\alpha(x-x_d)\}+f(y-y_d) & h(x,y)<0 \end{cases} \tag{20}$$

If the interface is parallel to the y-axis ($\alpha=0$), the second equation of Eq.20is replaced by Eq.21.

$$u_B^h=a+e(x-x_d)+c(y-y_d) \qquad h(x,y)<0 \tag{21}$$

The shape function for two-dimensional problems can then be obtained by following the same solution procedure for one-dimensional problems as shown in Eqs.22-24.

$$\begin{cases} \phi_I(\mathbf{x})=\mathbf{p}_1(\mathbf{x})^T(\mathbf{A}^{-1}\mathbf{B})_I & h(x,y)\geq 0 \text{ zone A} \\ \phi_I(\mathbf{x})=\mathbf{p}_2(\mathbf{x})^T(\mathbf{A}^{-1}\mathbf{B})_I & h(x,y)<0 \text{ zone B} \end{cases} \tag{22}$$

$$\mathbf{p}_1(x)=\begin{bmatrix} 1 \\ x-x_d \\ y-y_d \\ 0 \end{bmatrix} \tag{23}$$

$$\begin{cases} \mathbf{p}_2(x)=\begin{bmatrix} 1 \\ x-x_d \\ \alpha(x-x_d) \\ -\alpha(x-x_d)+y-y_d \end{bmatrix} & (\alpha\neq 0) \\ \mathbf{p}_2(x)=\begin{bmatrix} 1 \\ 0 \\ y-y_d \\ x-x_d \end{bmatrix} & (\alpha=0) \end{cases} \tag{24}$$

A and **B** in Eq.22 can be evaluated from Eqs.12, 13 respectively.

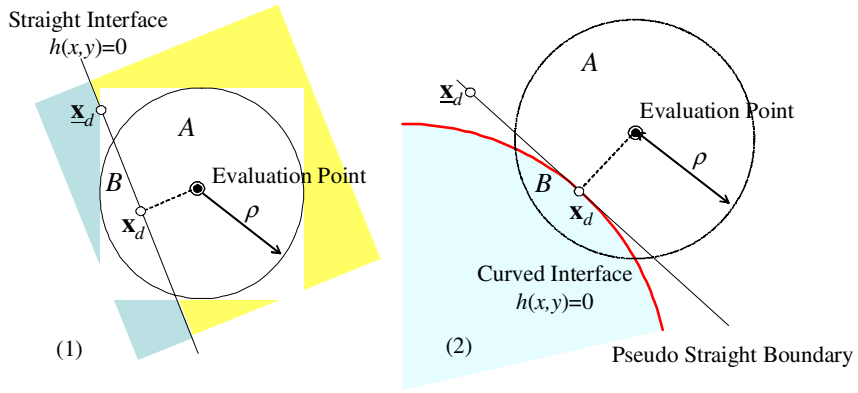

Figure 4 : Discontinuous derivative basis function for 2-D problems (Modeling of interface)

Fig. 5 compares shape functions and partial derivatives, in two-dimensional space on the straight interface, obtained by using MLSA with the discontinuous derivative basis function and those obtained by the conventional MLSA. It can be seen that the shape function obtained by the proposed technique captures the sharp peak at the interface, thus realizing derivative discontinuity along the interface.

For curved interfaces, the tangent line at x_d, the nearest point on the interface from the evaluation point, is regarded as the pseudo straight interface as shown in Fig. 4-2. The same procedure described above can also be applied. The validity of this technique is demonstrated in subsequent numerical examples.

4 Noted Observations of Proposed Technique

4.1 Number of sampling points and singularity of matrix A

If the number of sampling points in the domain of influence is not sufficient, the matrix **A** in Eqs.11, 22 becomes singular and cannot be inverted. For two-dimensional problems, where the number of unknown coefficients in Eqs.20, 21 is four, at least four sampling points are necessary in the domain of influence to determine the coefficient values. In addition, linear polynomial functions must be reproduced in both zones A and B as shown in Fig.4. At least three sampling points are required in each zone. Therefore to be able to invert **A** and evaluate the shape function, the minimum requirement demands for at least one sampling point within each zone and two on the interface shared by both zones. Should the domain of influence include the material beyond the interface and the number of sampling points in the other zone is not sufficient, the MLSA scheme is utilized only in the zone the evaluation point resides in.

4.2 Linear reproducing condition and convergence property

Completeness and compatibility are sufficient conditions for the convergence of a solution by Galerkin-type numerical methods. As the convergence of meshfree methods using conventional MLSA was already proven and discussed in literatures [8][15][16], only the linear reproducing condition of the proposed technique is investigated here. If the problem is homogeneous and the same material exists on both sides of the material interface, the function produced by the proposed MLSA using the discontinuous basis function must be identical to that produced by conventional MLSA. Although each function on both sides of the material interface possesses different slope values, as shown in Fig. 1, the same slope values can be obtained in the constant strain state as the method is based on the least squares approach. Therefore, the convergence property in homogeneous problems is assured and is also demonstrated in following numerical examples.

4.3 Comparison with other methods

The major difference that the proposed technique possess from conventional methods is that all sampling points in the domain of influence on both sides of the material interface are taken into account as shown in the Fig. 13. These sampling points on either side of the material interface improves the accuracy of the constants in Eqs.8, 20. However, for other methods, the domain of influence

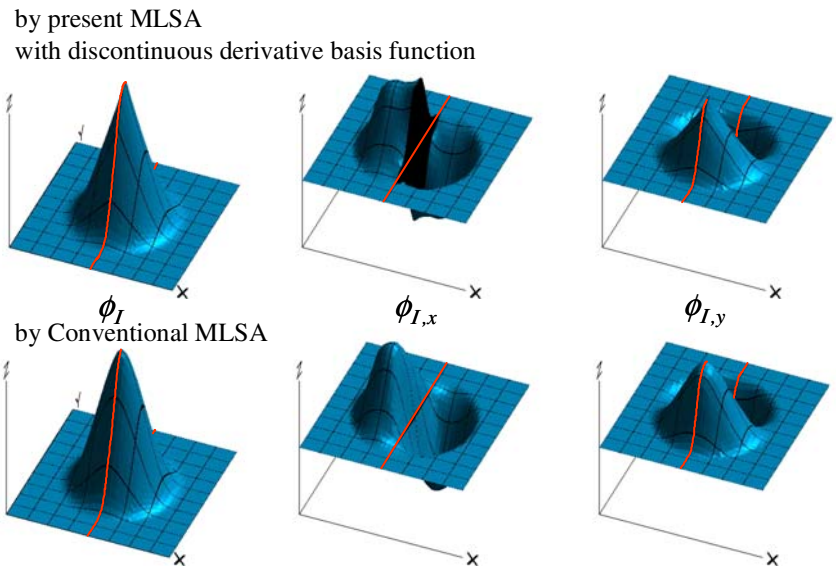

Figure 5 : Shape function and its partial derivative in space (2-D)

is truncated and the number of sampling points significantly decreases near the interface. The patch methods [Cordes and Moran (1996)] [Kawashima and Noguchi (2000)] [Noguchi and Kawashima (2004)], are simple and utilize Lagrange multipliers or the penalty method to impose displacement field continuity at the interface, suffer from stress and strain oscillations near the interface which require the application of smoothing schemes. The Enriched methods use a jump shape function [Krogauz and Belytschko (1998)] [Wang, Chen and Sun (2003)] that considers the discontinuity in derivatives of sampling points on the interface in order to improve accuracy. Although better results were obtained, it was also reported that the computed results depended on the parameter to determine the shape of the jump function. Furthermore, in case of the method by Krongauz et al., additional degrees of freedom may be required to determine the amplitude of the jump function in the global system of equations, which complicates the formulation for two-dimensional problems. The proposed technique has no parameter dependency as no jump shape function is introduced and therefore requires no additional degrees of freedom. Furthermore, by comparing basis vector Eqs.2, 23-24, it can be seen that, for two-dimensional problems, the proposed discontinuous basis function requires only an additional coefficient to determine the local value of the approximated displacement function as compared to three coefficients when using the conventional linear basis function in MLSA. Therefore the proposed technique is computationally efficient when compared to the conventional linear basis function.

5 Numerical Examples

For the following examples, the EFG method [Gu and Liu (2001)] is used where MLSA is utilized for spatial discretization. Essential boundary conditions are imposed by the penalty method. For domain integration, background cells and 6 x 6 Gauss quadratures are used.

Several numerical analyses are conducted to demonstrate the effectiveness of the proposed method. Results for both one-dimensional and two-dimensional problems with bi-material properties are presented. One-dimensional problems include a rod subjected to tensile loads and a rotating disk subjected to radial loads. Two-dimensional problems include a cantilever beam problem subjected to shear loading and a circular inclusion with uniform eigen strain in an infinite plate. These are typical problems, which have already been solved in past studies [Cordes and Moran (1996)] [Kawashima and Noguchi (2000)] [Krogauz and Belytschko (1998)] [Wang, Chen and Sun (2003)]. The results obtained by the proposed technique are all compared with their known exact solutions. The abbreviations “DBF” and “No DBF” in Figs. 7-15 represent the proposed technique, MLSA with the discontinuous basis function, and conventional MLSA

methods respectively.

5.1 One-dimensional problems

5.1.1 Bi-material rod

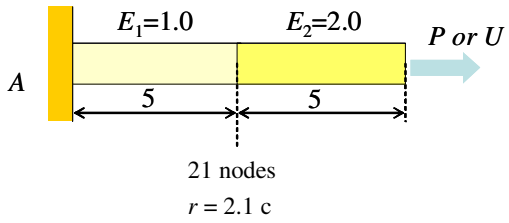

Figure 6 : 1-D bi-material rod

Fig. 6 shows a one-dimensional rod consisting of two materials with elastic moduli E_1=1 and E_2=0.5. One end is fixed and the other is subjected to tensile load. The length of the bar L=10; the cross-sectional area A is constant and equal to 1. The material interface is at x = 5. The analysis is carried out using 21 uniformly spaced nodes with integrated cells demarcated by the nodes. The size of the domain of influence is $2.1c$, where c denotes the minimum distance between distributed nodes.

Two separate cases are conducted. For the first case, a unit tensile force P= 1 is applied. The analytic solution is evaluated by establishing axial force equilibrium and is shown in Eq.25.

$$\varepsilon(x) = \begin{cases} P/AE_1, & x \le 5 \\ P/AE_2, & x \ge 5 \end{cases} \tag{25}$$

Fig. 7 compares the axial strains, at Gaussian points, evaluated by the proposed DBF technique and conventional linear basis function. It can be seen that the solution of DBF are match with the exact solution whereas the conventional method gives an oscillating solution near the material interface. In fact, the proposed technique gives exact solution for this problem, because DBF is able to represent bi-linear functions. It is noted that when a bi-linear function is utilized as the basis function for MLSA, two different-valued and discontinuous derivatives can be evaluated simultaneously on the interface.

For the second case, a prescribed displacement of u = 1 and a body force $b(x) = x$ are applied. This problem was solved by Krongauz et al. [Krogauz and Belytschko

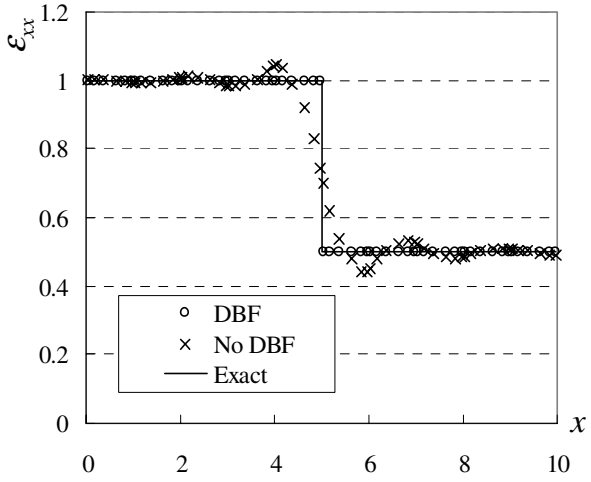

Figure 7 : Comparison between axial strains of 1-D bi-material rod with unit tensile force

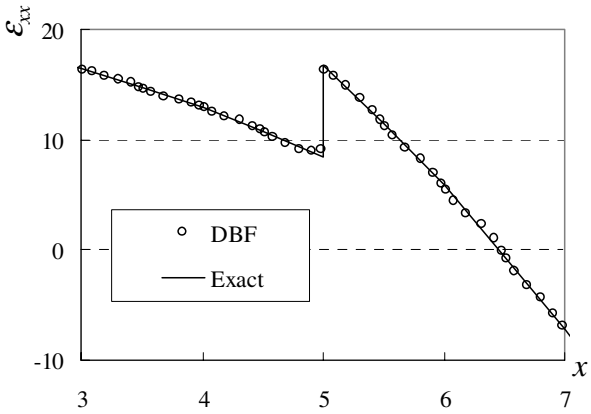

Figure 8 : Comparison between axial strains of 1-D bi-material rod with tensile and body force

(1998)]. The analytic solution for this case is shown in Eq.26.

$$\varepsilon(x) = \begin{cases} \frac{1}{E_1}\left(CE_2 - \frac{x^2}{2}\right), x \le 5 \\ C - \frac{x^2}{2E_2}, x \ge 5 \end{cases},$$
$$C = \frac{6E_1E_2 + 875E_1 + 125E_2}{30E_2(E_1 + E_2)} \tag{26}$$

Fig. 8 shows a magnified view of the strains around the discontinuity for the second case, which are plotted at the Gaussian points. By using DBF, a highly accurate

solution is obtained with the strain jump at the material interface being captured.

5.1.2 Bi-material rotating disk

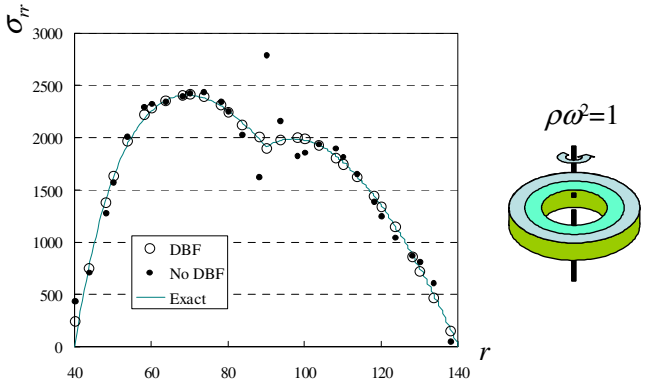

Figure 9 : Comparison between radial stresses of 1-D rotating disc with centrifugal force

This analysis solves the same problem that in [Kawashima and Noguchi (2000)], where the exact solution was given. Due to axis symmetry, boundary conditions are not required and the effects from imposing them are not included. The rotating disk consists of two materials with elastic moduli E_1=1000 and E_2=2000. The radius of the cavity is 40 and that of the disk is 140. Fig. 9 shows the material interface at x = 90. A unit centrifugal force PΩ^2 is applied. Computations were made using 11 uniformly spaced nodes with the integrated cells demarcated by the nodes. The size of the domain of influence is 4.1c.

For this problem, radial stresses and hoop strains are continuous while hoop stresses and radial strains are discontinuous. Fig. 9 shows the exact solution and the computed radial stresses which are plotted at the Gaussian points. It can be seen from Fig. 9 that the proposed technique has better accuracy than the conventional method, whose results oscillate around the material interface.

5.2 Two-dimensional problems

5.2.1 Cantilever beam problem

Two two-dimensional cantilever beam examples will be presented in this section. An inhomogeneous cantilever beam example will be presented first, followed by a homogeneous cantilever beam example. Both of which are

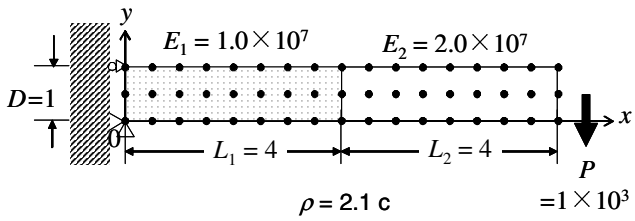

Figure 10 : Cantilever beam with shear end load

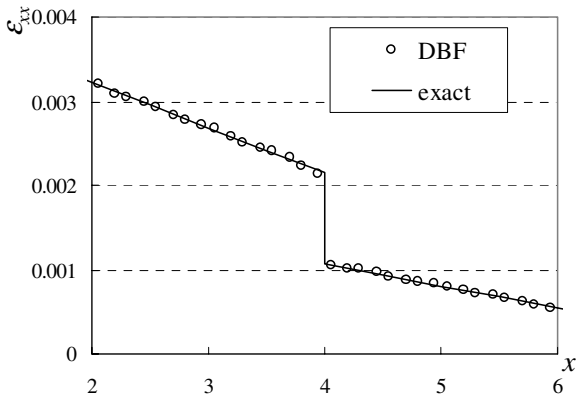

Figure 11 : Comparison between axial strains of cantilever beam with shear end load

subjected to shear loading. For the former, a cantilever beam consisting of two materials with elastic moduli E_1=1.0x10^7 and E_2=2.0x10^7 is analyzed by the proposed technique. The length of the beam L_1+L_2=8; the height D and the thickness are constant and equal to 1. The material interface is located at x = 4. The beam is fixed on one end and shear force is applied on the other end as shown in Fig. 10. The analysis is conducted with 51 uniformly spaced nodes, with integrated cells demarcated by the nodes. The size of the domain of influence is 2.1c.

Fig. 11 compares strain values that are plotted at Gaussian points nearest to the top surface of the beam, in the direction of the x-axis, obtained by the proposed technique and of the known exact solution. The exact distribution of strain in the x direction is given in Eq.27 [Kawashima and Noguchi (2000)].

$$\begin{cases} \varepsilon_{xx} = -\frac{12p}{D^3E_1}(L_1+L_2-x)(y-\frac{1}{2}D) \\ \qquad\qquad (0 \le \mathrm{x} \le L_1) \\ \varepsilon_{xx} = -\frac{12p}{D^3E_1}(L_1+L_2-x)(y-\frac{1}{2}D) \\ \qquad\qquad (L_1 < \mathrm{x} \le L_1+L_2) \end{cases} \tag{27}$$

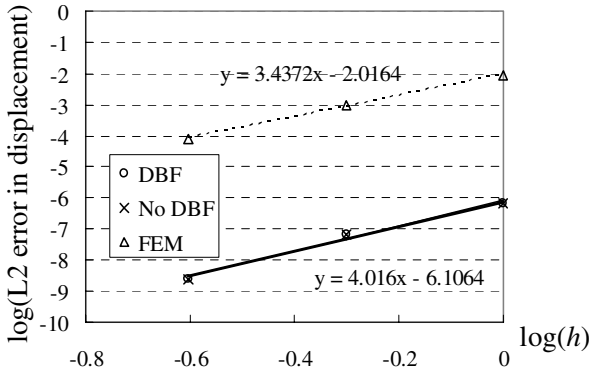

Figure 12 : Convergence rates in L2 norm of error in displacements for cantilever beam with shear end load

The proposed technique gives a highly accurate solution and captures the strain discontinuity at the interface.

The second example considers a two-dimensional homogeneous cantilever beam. The analysis conditions are the same as the previous case, except that the value of Young's modulus is the same for each material. The objective of this example is to investigate the linear

reproducing property of the proposed technique and the convergence of L_2 displacement norm. The norm is calculated according to Eq.28 and the exact solution is available in [Belytschko, Lu and Gu (1994)] and [Kawashima and Noguchi (2000)].

L_2 displacement norm

$$= \{ \int_{\Omega} (\mathbf{u}^{NUM} - \mathbf{u}^{EXACT})^T (\mathbf{u}^{NUM} - \mathbf{u}^{EXACT}) d\Omega \}^2 \quad (28)$$

The convergence plot is illustrated in , where results by EFG and FEM are shown. The discontinuous basis function has been introduced in this example around the interface, which is not necessary for homogenous problems, to check the linear reproducing property of the proposed technique. Fig. 12 shows that the convergence rate of the proposed technique coincides with that of EFG, which uses the linear basis function in MLSA. It also shows that both convergent rates are superior to that of FEM. Therefore there is no disadvantage even if the proposed technique is adopted to solve homogeneous problems.

5.2.2 *Inclusion in an infinite plate*

The proposed technique is applied here to solve a problem that involves a circular inclusion in an infinite plate. The inclusion is subjected to a constant dilational eigenstrain ε^q, such as a transformation or thermal strain. Fig. 13 shows the model that is used for analysis. This problem has been solved by several past studies [Cordes and Moran (1996)] [Kawashima and Noguchi (2000)] [Krongauz and Belytschko

(1998)] and the analytical solution with no body force was given by Eqs.29-30.

$$u_r(r) = \begin{cases} C_1 r, \ r \le R \\ C_1 R^2 / r, \ r \ge R \end{cases} \quad (29)$$

$$u_\theta = 0 \quad (30)$$

The exact strains are given by Eqs.31-34.

$$\varepsilon_{rr}(r) = \begin{cases} C_1, \ x < R \\ -C_1 R^2 / r^2, \ x > R \end{cases} \quad (31)$$

$$\varepsilon_{\theta\theta}(r) = \begin{cases} C_1, \ x \le R \\ C_1 R^2 / r^2, \ x \ge R \end{cases} \quad (32)$$

$$\varepsilon_{r\theta}(r) = 0 \quad (33)$$

$$C_1 = \frac{(\mu_1 + \lambda_1)\varepsilon_1^*}{\mu_1 + \lambda_1 + \mu_2} \quad (34)$$

μ and λ are Lame constants of the materials and the relationships between Young's modulus and Poisson's ratio are written as Eqs.35-36.

$$\lambda = \frac{\nu E}{(1+\nu)(1-2\nu)} \quad (35)$$

$$\mu = G = \frac{E}{2(1+\nu)} \quad (36)$$

For this analysis, subscript 1 denotes the inclusion and 2 denotes the surrounding material. The material properties used for this analysis are E_1=1000, ν_1=0.28 and E_2=900, ν_2=0.33. Due to symmetric properties, only a quarter of the model was analyzed. The nodal arrangement around the inclusion is also shown in Fig. 13. The total number of nodes is 897, out of which 88 nodes are in the inclusion and 13 on the interface. The size of the domain of influence is $2.8c$ and the constant dilational eigenstrain is defined as ε_x^q=1.

Figs. 14 and 15(a-b) compare the results obtained by the proposed technique and the exact solution along the

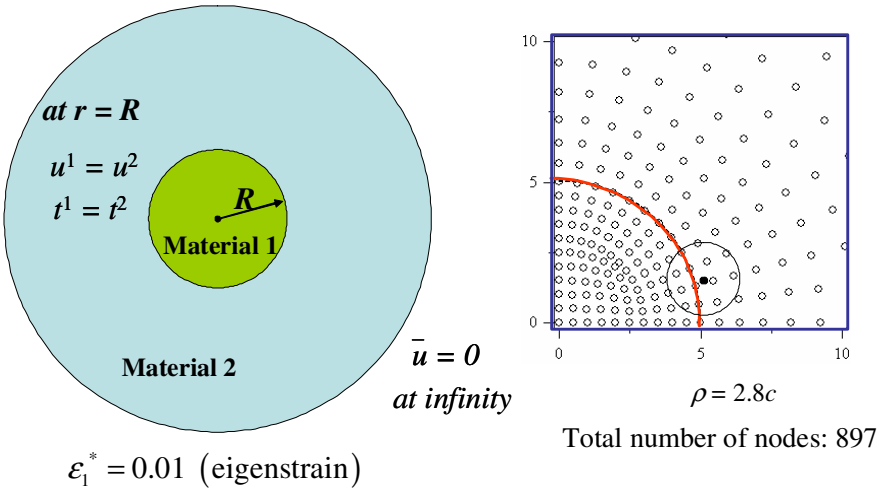

Figure 13 : Inclusion in infinite plate with constant eigenstrain

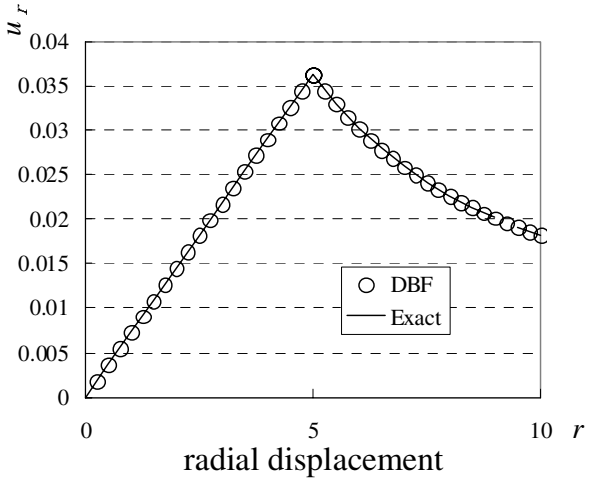

Figure 14 : Comparison between radial displacements of inclusion in infinite plate

plate's radius. As can be seen from those figures, radial displacement and hoop strain are continuous but the radial strain is discontinuous at the material interface. Fig. 14 shows that for the radial displacement, the obtained results completely agree with the exact solution. It can be seen that the sharp edge along the interface is produced by the proposed technique. Fig. 15(a) shows results of radial strain obtained by the proposed technique, which matches the exact solution. It also shows oscillations around the interface when the conventional linear basis function is used. Fig. 15(b) shows that both the proposed technique and the conventional method perform well when computing hoop strains.

5.2.3 *Homogenization analysis for CFRP*

Modeling material interface properly is essential for analysis of composites. The proposed technique is applied here to homogenization method [Guedes and Kikuchi (1990)] for quasi 3-dimensional analysis of composites to compute homogenized elastic moduli. The analysis model considered is Carbon Fiber Reinforced Plastic (CFRP) and its properties are illustrated in Fig. 16. The radius of fiber and the volume fraction are varied as Table 1. The homogenized elastic constants which are calculated as components of effective constitutive matrix **D** (Eq.37) are compared with the properties Halpin-Tsai theory [Halpin and Kardos (1976)].

$$\mathbf{D} = \begin{bmatrix} E_{11} & E_{12} & E_{13} & & & \\ E_{21} & E_{22} & E_{23} & & & \\ E_{31} & E_{32} & E_{33} & & & \\ & & & G_{23} & & \\ & & & & G_{31} & \\ & & & & & G_{12} \end{bmatrix} \tag{37}$$

The properties are calculated in the theory as follows. For E_{33}, Eq.38 is adopted.

$$E_{33} = E_f V_f + E_m V_m \tag{38}$$

where V is volume ratio, f represents fiber and m represents matrix. The other properties are calculated using Eqs.39, 40.

$$M = M_m \frac{1 + \xi\eta V_f}{1 - \eta V_f} \tag{39}$$

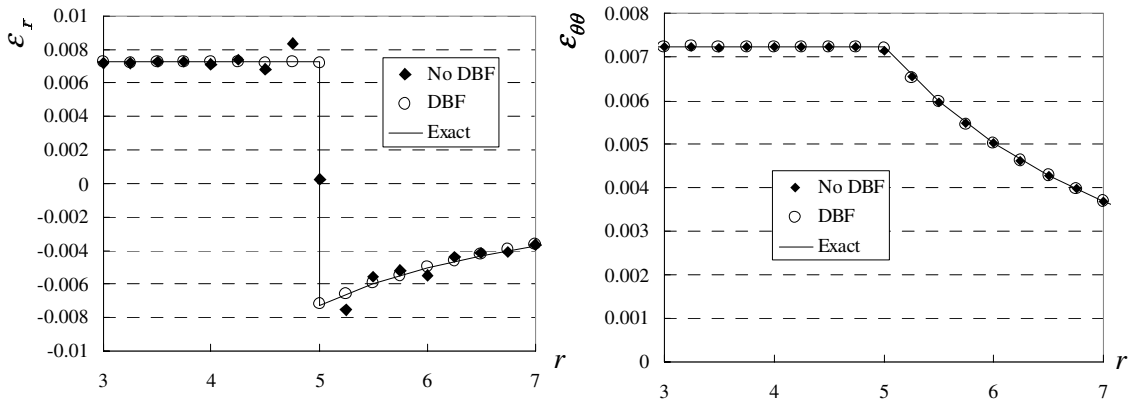

(a) radial strain (b) hoop strain

Figure 15 : Comparison between radial & hoop strains of inclusion in infinite plate

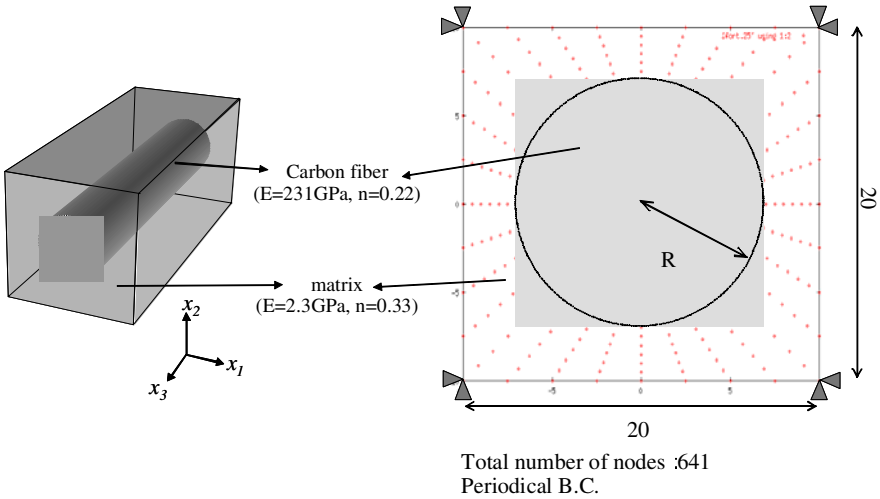

Figure 16 : Analysis model of composite (Carbon fiber reinforced plastic)

$$\xi = \begin{cases} 2 & (M = E_{11},\ E_{22}) \\ 1 & (M = G) \end{cases}, \quad \eta = \frac{M_f/M_m - 1}{M_f/M_m + \xi} \tag{40}$$

Fig. 17 shows results of homogenized elastic constants obtained by the proposed technique, which agree with the solution of Halpin-Tsai theory well.

6 Discussion and conclusions

This paper proposed a novel, simple and accurate technique for modeling discontinuous derivatives in meshfree methods for the analysis of structures with material interfaces. The novel discontinuous basis function (DBF) was introduced into the existing MLSA scheme replacing the conventional linear basis function. Comparing with recent methods, the proposed technique stands out because its domain of influence is not truncated at the interface and it utilizes all nodal information in the domain of influence. Furthermore, no strain jump function or additional global degrees of freedom are required nor included in the formulation. Therefore, this new technique can be easily incorporated into existing meshfree methods based on the MLSA scheme, such as the EFG method. Several successful numerical examples of 1-D and 2-D structures with material interfaces were also presented.

However, the proposed technique assumes the pseudo straight material interface when dealing with curved interfaces. But sufficient and accurate results were obtained when dealing with such cases as shown in the numerical examples. Future endeavors will include the application of the proposed technique to more compli-

Table 1 : Radius of fiber and volume fraction

R (radius of fiber)	4	5	6	7	8	9
V_f (Volume Fraction)	0.125	0.196	0.282	0.384	0.502	0.636

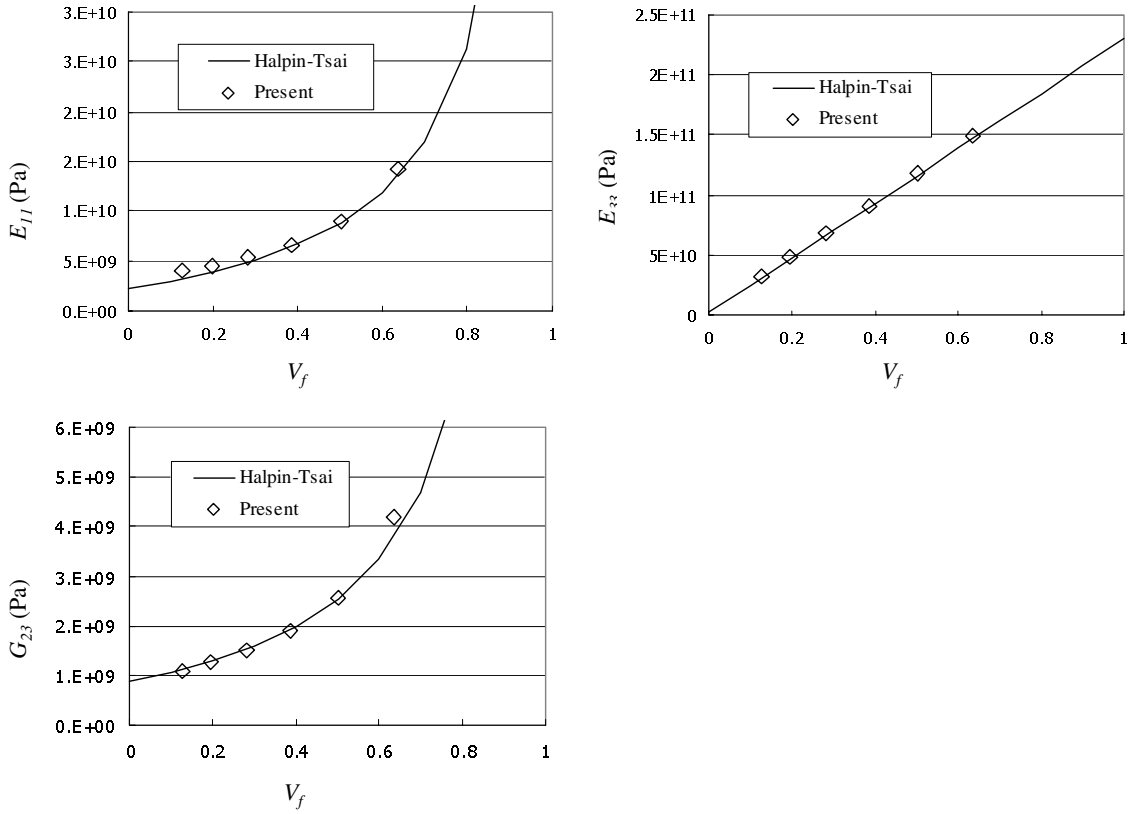

Figure 17 : Comparison between homogenized elastic constants and the properties of Halpin-Tsai theory

cated problems, such as arbitrary curved material interfaces and interfaces with junctions made of multiple materials. The extension of this technique to 3-D structural analysis is also a future issue yet to be developed.

Acknowledgement: This study is partly supported by Grant in Aid for the 21st century Center of Excellence (21^{st} COE) for "System Design: Paradigm Shift from Intelligence to Life" from Ministry of Education, Culture, Sport, and Technology in Japan. The authors greatly acknowledge the support.

References

Atluri, S.N. (2004): *The Meshless Local-Petrov-Galerkin Method for Domain & BIE Discretizations*. Tech Science Press, Forsyth, GA.

Atluri, S. N.; Zhu, T. (1998): A new meshless local Petrov-Galerkin (MLPG) approach in computational mechanics. *Computational Mechanics*, vol. 22, pp. 117-127.

Belytschko, T.; Lu, Y. Y.; Gu, L. (1994): Element-free Galerkin methods. *Int. J. Num. Meth. Engrg.*, vol. 37, pp. 229-256.

Cordes, W.; Moran, B. (1996): Treatment of material discontinuity in the element-free Galerkin method. *Comput. Meth. Appl. Mech. Engrg,* vol. 139, pp. 75-89.

Dilts, **G. A.** (1999): Moving-least-squares-particle hydrodynamics I. Consistency and stability. *Int. J. Numer. Meth. Eng.,* vol. 44, pp. 1115- 1155.

Duarte, C. A.; Oden, **J. T.** (1996): An h-p adaptive method using clouds. *Comp. Meth. Appl. Mech. Engrg.*,

vol. 139, pp. 237-262.

Gu, Y. T.; Liu, G. R. (2001): A local point interpolation method (LPIM) for static and dynamic analysis of thin beams. *Computer Methods in Applied Mechanics and Engineering,* vol. 190, pp. 5515-5528.

Guedes, J. M.; Kikuchi, N. (1990): Preprocessing and postprocessing for materials based on the homogenization method with adaptive finite element methods. *Comper Methods in Applied Mechanics and Engngineering*, vol. 83, pp. 143-198.

Halpin, J. C.; Kardos, J. L. (1976): The Halpin Tsai eqations: A rewiew. *Polymer Engineering and Science*, vol. 16, pp.334-352.

Kawashima, T.; Noguchi, H. (2000): Mesh free analyses of Structures with discontinuous field using EFGM. *Trans. JSME (Category-A) in Japanese*, vol. 66, pp. 1786-1793.

Krongauz, Y.; Belytschko, **T.** (1996): Enforcement of essential boundary conditions in meshless approximations using finite elements. *Computer Methods in Applied Mechanics and Engineering,* vol. 131, pp. 133-145.

Krongauz, Y.; Belytschko, T. (1998): EFG approximation with Discontinuous Derivatives. *Int. J. Num. Meth. Engrg,* vol. 41, pp. 1215-1233.

Krysl, P.; Belytschko, T. (1997): Element-Free Galerkin Method: Convergence of the Continuous and Discontinuous Shape Functions. *Computer Methods in Applied Mechanics and Engineering,* vol. 148, pp. 257-277.

Li, Q.; Shen, S.; Han, Z. D.; Atluri, S. N. (2003): Application of Meshless Local Petrov-Galerkin (MLPG) to Problems with Singularities, and Material Discontinuities, in 3-D Elasticity. *CMES: Computer Modeling in Engineering and Sciences*, Vol. 4, No. 5, pp. 571-586.

Lin, H.; Atluri, S. N. (2000): Meshless Local Petrov-Galerkin (MLPG) Method for Convection-Diffusion Problems, *CMES: Computer Modeling in Engineering and Sciences*, Vol. 1, No. 2, pp. 45-60

Liu, G. R. (2002): Mesh Free Methods: Moving Beyond the Finite Element Method, CRC Press.

Liu, W. K.; Jun, S.; Zhang, Y. F. (1995): Reproducing kernel particle methods. *Int. J. Num. Meth. Fluid*, vol. 20, pp. 1081-1106.

Monaghan, **J. J.** (1982): An introduction of SPH. *Computer Physics Communications*, vol. 48, pp. 89-96.

Nayroles, B.; Touzot, G.; Villon, **P.** (1992): Generalizing the finite element method: diffuse approximation and diffuse elements. *Computational Mechanics*, vol. 10, pp. 307-318.

Noguchi, H.; Kawashima, T. (2004): Meshfree analyses of cable reinforced membrane structures by ALE-EFG method. *Engineering Analysis with Boundary Elements*, vol. 28, pp. 443-451.

Wang, D.; Chen, J. S.; Sun, L. (2003): Homogenization of magnetostrictive particle-filled elastomers using an interface-enriched reproducing kernel particle method. *Finite Elements in Analysis and Design*, vol. 39, pp. 765-782.